JOURNAL OF THERMOPHYSICS AND HEAT TRANSFER
Vol. 21, No. 1, January–March 2007

Analysis of Diffusion Phenomena in CO_2/N_2 Mixtures under Thermochemical Equilibrium

P. Rini,* D. Vanden Abeele,† and G. Degrez‡
von Karman Institute for Fluid Dynamics (VKI), 1640 Rhode-St.-Genèse, Belgium
Université Libre de Bruxelles (ULB), 1050 Bruxelles, Belgium

DOI: 10.2514/1.23471

In this paper we apply a recently published formulation of the equations governing the behavior of local thermodynamic equilibrium flows, accounting for the variation in local elemental concentrations in a rigorous manner, to simulate heat and mass transfer in the boundary layer near the stagnation point of a hypersonic vehicle entering the Martian atmosphere. The results obtained using this formulation are compared with those obtained using a previous form of the equations where the diffusive fluxes of elements are computed as a linear combination of the species diffusive fluxes. This not only validates the new formulation used in this contribution but also highlights its advantages with respect to the previous one: by using and analyzing the full set of equilibrium transport coefficients we arrive at a deep understanding of the mass and heat transfer for a CO_2/N_2 mixture.

Nomenclature

D_{eq}	=	elemental multicomponent diffusion coefficient of element e with respect to element q
D^T_{eq}	=	elemental thermal demixing diffusion coefficient of element e
h	=	mixture enthalpy per unit mass
h_s	=	enthalpy of species s
R_m	=	radius of the probe hold in the test chamber
r	=	local radius of the probe
u	=	component of the velocity in the x direction
v	=	component of the velocity in the y direction
x	=	physical coordinate along the body contour
y	=	physical coordinate normal to the body
η	=	second Lees–Dorodnitsyn coordinate
μ	=	dynamic viscosity
ξ	=	first Lees–Dorodnitsyn coordinate

Subscripts

w	=	wall
δ	=	boundary layer edge

Presented as Paper 3790 at the 9th AIAA/ASME Joint Thermophysics and Heat Transfer Conference, Hyatt Regency San Francisco at Embarcadero Center San Francisco, California, 5–8 June 2006; received 25 February 2006; revision received 25 April 2006; accepted for publication 26 April 2006.

*Assistant at the ULB, Service de Mécanique des Fluides, Avenue F. Roosevelt, 1050, Bruxelles; also Ph. D. Candidate at the VKI, Department of Aeronautics and Aerospace, 72, Chaussée de Waterloo, 1640, Rhode-St.-Genése, Belgium; rini@vki.ac.be. Member AIAA.

†Researcher Engineer at the VKI, Department of Aeronautics and Aerospace, 72, Chaussée de Waterloo, 1640, Rhode-St.-Genése, Belgium; also Assistant at the ULB, Service de Mécanique des Fluides, Avenue F. Roosevelt, 1050, Bruxelles; david.vanden.abeele@vki.ac.be. Member AIAA.

‡Adjunct Professor at the VKI, Department of Aeronautics and Aerospace, 72, Chaussée de Waterloo, 1640, Rhode-St.-Genése, Belgium; also Professor at the ULB, Service de Mécanique des Fluides, Avenue F. Roosevelt, 1050, Bruxelles, Belgium; gdegrez@ulb.ac.be. Associate Fellow AIAA.

Introduction

THE physics of collision-dominated chemically reacting flows is described by an extended Navier–Stokes system, consisting of the following equations [1]: 1) global continuity, momentum, and total energy; 2) a separate continuity equation for each species, including finite-rate chemistry; 3) if thermal nonequilibrium occurs, an energy equation for each additional mode of freedom (vibrational, rotational, and electronic energies). This formalism is widely employed for the simulation of high temperature flow conditions typical of both atmospheric entry and ground tests performed in high enthalpy facilities. In general, after very complex and costly computations, the solution of the previous equations leads to a vast amount of information (e.g., concentration fields of a large number of chemical species) whose interpretation may by no means be obvious. In addition many physical parameters essential for the modeling of chemistry and energy relaxation processes are required to close the previous system of equations. Unfortunately, in most applications, accurate estimations of these parameters are missing affecting in general the uncertainty of the obtained prediction. For these reasons, when chemistry and energy exchanges are fast, it is usually preferable to solve the more elegant local thermochemical equilibrium (LTCE) form of the aforementioned set of equations.

A major breakthrough in the field of LTCE flow modeling was made by Butler and Brokaw [2,3], who showed that, assuming vanishing diffusive fluxes of chemical elements, the diffusive transport of species reaction enthalpies in the energy equation could be incorporated in a straightforward manner by introducing a coefficient of "thermal reactive conductivity" λ_R:

$$\mathbf{q}_d = \sum_{s=1}^{N_{sp}} \mathbf{J}_s h_s = -\lambda_R \nabla T \tag{1}$$

One often makes use of this result to reduce the full set of nonequilibrium equations to a system formally equivalent to the "conventional" Navier–Stokes equations (continuity, momentum, and energy), complemented by a modified equation of state $\rho(p, T)$ computed from statistical mechanics assuming a fixed elemental composition in the flow [4].

Although appealing because of its simplicity, it is important to understand that this approach is approximate at best, because in general the elemental composition varies significantly in chemically reacting flows [5,6].

Over the past four decades, several LTCE formulations accounting to some extent for (de)mixing effects have been proposed [7–13]. Recently, the present authors presented a new formalism [14] which has the advantage that elemental fluxes and

diffusion heat fluxes are explicitly expressed as a function of the temperature and elemental mass fraction gradients.

In this paper we present the full set of equilibrium transport coefficients introduced in [14] for an 8 species mixture containing three elements (C, N, O) of interest for Mars entry. The numerical results, discussed at the end of the manuscript, show the main advantages of the formulation proposed in [14] and, in particular, allow the achievement of the main objectives of this study stated hereafter.

1) The application of the formulation proposed in [14] to a mixture containing three elements proves definitely its general character with respect to previous formulations available in the literature.

2) The computation of thermal demixing coefficients as well as elemental multicomponent diffusion coefficients allows for the accurate and exhaustive description of diffusion phenomena in mixtures of reacting gases under LTCE. In particular, inspired by the structure of the multicomponent matrix, we propose an approximate method to predict a priori the evolution of the elemental fraction profiles along the stagnation line.

3) A more general expression for the LTCE heat flux vector is proposed which represents a generalization of the Butler and Brokaw formula. By computing the correction to λ_R as well as the elemental heat-transfer coefficients, a deep understanding of enthalpy transport by diffusion is achieved.

In the remaining part of this paper we first recall the main aspects of the LTCE formulation derived by the authors in [14]. Then we apply this formulation to the stagnation line problem, which represents a building block of the methodology [15] used at the von Karman Institute (VKI) to estimate the catalytic properties of thermal protection system (TPS) materials. Finally we discuss the results of the stagnation line problem for a CO_2/N_2 mixture, presenting a deep analysis of both mass and energy transfer thanks to the knowledge of the new transport properties introduced.

Species Ordering and Nomenclature

We represent mixtures of ideal gases by means of a finite set of N_{sp} species $\mathcal{S}$, among which we further distinguish between N_c "independent species" $\mathcal{E}$ consisting of pure elements and N_r "combined species" $\mathcal{R}$ and $\mathcal{S} = \mathcal{R} \cup \mathcal{E}$. We characterize the chemical composition of the mixture by means of mole fractions $x_s = n_s/n$, where n_s and n stand for the molar densities of individual species and of the entire mixture. Alternatively, we also characterize the mixture composition by means of the mass fraction $y_s = \rho_s/\rho$, where ρ_s and ρ stand for the mass densities of the individual species, respectively, the full mixture.

We will indicate the number of elements e contained in a species s by ϕ_s^e, for instance, for NO, $\phi_{\mathrm{NO}}^{\mathrm{N}} = 1$, while for CO_2, $\phi_{\mathrm{CO_2}}^{\mathrm{O}} = 2$. This allows for the definition of the mass fractions Y^e of elements in the mixture as follows:

$$Y^e = \sum_{s\in\mathcal{S}} \phi_s^e y_s \frac{M_e}{M_s} \qquad (e \in \mathcal{E}) \tag{2}$$

where M_s is the molar mass of species s, related to the mixture molar mass $M = \sum_{s\in\mathcal{S}} x_s M_s$. Alternatively we can characterize the elemental composition in terms of mole fractions (X^e) which are linked to the mass fractions by a relation similar to the one holding for the mixture species, that is, $Y^e = X^e M_e / \sum_{e\in\mathcal{E}} M_e X^e$. We introduce the diffusion velocity $\mathbf{V}_s$ with respect to the mass-averaged velocity of the mixture $\mathbf{u}$. The mass fluxes of species s are then given by, respectively, $\mathbf{J}_s = \rho_s \mathbf{V}_s$ and the diffusive mass fluxes of element e are obtained from the following linear combination:

$$\mathcal{J}_e = \sum_{s\in\mathcal{S}} \phi_s^e \mathbf{J}_s \frac{M_e}{M_s} \qquad (e \in \mathcal{E}) \tag{3}$$

Mixture Composition Under LTCE

Species Continuity Equations

We consider the commonly encountered flow regime in which chemical reactions are relatively rare with respect to elastic collisions, such that they do not play an important role in the thermalization of species in the flow (unlike the "kinetic chemical equilibrium regime" considered in the first part of [16], for which chemical reactions and elastic collisions are treated on the same level). The concentration of each species may then be determined from a respective species continuity equation [1]:

$$\partial_t(\rho y_s) + \nabla\cdot(\rho y_s \mathbf{u}) + \nabla\cdot\mathbf{J}_s = \dot{\omega}_s \tag{4}$$

where $\mathbf{u}$ stands for the mass-averaged velocity of the mixture and $\dot{\omega}_s$ is the mass production/destruction term [17] of species s due to chemical reactions. The number fluxes of species respect the mass conservation constraint

$$\sum_{s\in\mathcal{S}} \mathbf{J}_s = 0 \tag{5}$$

and obey the Stefan–Maxwell equations

$$\frac{M}{\rho}\sum_{j\in\mathcal{S}}\left(\frac{x_s\mathbf{J}_j}{M_j\mathcal{D}_{sj}f_{sj}(L)} - \frac{x_j\mathbf{J}_s}{M_s\mathcal{D}_{sj}f_{sj}(L)}\right) = \nabla x_s \qquad (s \in \mathcal{S}) \tag{6}$$

In the present study we have neglected effects of pressure and thermal diffusion [18,19]. The binary diffusion coefficients $\mathcal{D}_{sj}$ are symmetric $\mathcal{D}_{sj} = \mathcal{D}_{js}$ and the symmetric factor $f_{sj}(L)$ takes into account the contribution of Laguerre–Sonine polynomials [20–23].

The binary diffusion coefficients can be further expressed as a function of the collision integrals for which detailed information is available in [24,25] for air and CO_2 and for the mixture used in this manuscript in [26,27].

Elemental Continuity Equations for Neutral Mixtures

As pointed out Suslov et al. [7] and later by Murphy [11], we need to solve additional element advection–diffusion equations to determine the elemental composition of the mixture [5]. To obtain these equations, we multiply Eq. (4) by $\phi_s^e M_e/M_s$ and sum over all species. Because no elements are created in chemical reactions, the mass fraction of any element e obeys the following equation:

$$\partial_t(\rho Y^e) + \nabla\cdot(\rho\mathbf{u}Y^e) + \nabla\cdot\mathcal{J}_e = 0 \qquad (e \in \mathcal{E}) \tag{7}$$

Equation (7) is valid regardless of the degree of chemical nonequilibrium of the mixture. In particular, under LTCE, the solution of the set of elemental continuity equations provides the mixture local elemental composition necessary to compute the mixture composition.

Elemental Diffusion Coefficients

As shown in [14], in a neutral reacting gas under local thermochemical equilibrium, at constant pressure, the elemental fluxes $\mathcal{J}_e$ are in general nonzero and can be explicitly expressed as a function of the gradients of temperature and elemental composition, that is,

$$\mathcal{J}_e = -\sum_{q\in\mathcal{E}} \rho D_{eq}\nabla Y^q - \rho D_e^T \nabla T \tag{8}$$

By combining Eqs. (7) and (8), we can write the elemental continuity equations as follows:

$$\partial_t(\rho Y^e) + \nabla\cdot(\rho\mathbf{u}Y^e) - \nabla\cdot\left(\rho\sum_{q\in\mathcal{E}} D_{eq}\nabla Y^q\right) = \nabla\cdot(\rho D_e^T\nabla T) \tag{9}$$

An important insight in the physical description of LTCE flows is highlighted by Eq. (9). There it is clearly shown that in a flow at LTCE, initially even at rest and with a uniform elemental distribution, in the presence of a temperature gradient sufficiently high to induce a gradient in species concentration, the elemental composition will in general vary in time and in space.

Diffusive Transport of Enthalpy

In a general nonequilibrium case, to compute the diffusive transport of enthalpy [Eq. (1)] one should determine all the $\mathbf{J}_s$ as solutions of Eq. (6) and then consider their linear combination. On the other hand, under thermochemical equilibrium, Eq. (1) takes a particular form which avoids the computation of the $\mathbf{J}_s$. A first step in this direction was done by Butler and Brokaw [2], who showed that, under the assumption of vanishing elemental fluxes, the diffusive heat flux takes the form of Eq. (1). In [1], the possibility of nonzero elemental fluxes is correctly taken into account and a more general expression for Eq. (1) is derived. Indeed, as shown in [14], for a mixture of reacting gases under thermochemical equilibrium, at constant pressure, the diffusive heat flux is proportional to both temperature and elemental concentration gradients as well:

$$\sum_{s\in\mathcal{S}} \mathbf{J}_s h_s = -(\lambda_R + \lambda_D)\nabla T - \sum_{e\in\mathcal{E}} \lambda^e_{\mathrm{EL}} \nabla Y^e \tag{10}$$

where λ_R is the reactive thermal conductivity introduced by Butler and Brokaw [2], λ_D is the demixing thermal conductivity which corrects for the inconsistent assumption of vanishing elemental fluxes, and, finally, the λ^e_{EL} are the elemental heat transfer coefficients. Analytical expressions for the LTCE transport properties are given in [14].

Thanks to the theoretical results recalled in the previous two sections, the full system of the governing equations of chemically reacting gases under LTCE can hence be reduced to a system formally equivalent to the conventional Navier–Stokes equations, extended with a set of N_c additional advection–diffusion equations, one for each of the mixture elements. By writing the governing equations of chemically reacting flows under LTCE in this way, the elements diffusive fluxes and the diffusive enthalpy flux depend in an explicit manner on the solution unknowns, which is advantageous for their implementation in an implicit CFD code. Moreover, the physical effects leading to (de)mixing and its influence on the mixture energetic behavior clearly show up. In the following section, we apply this formalism to a quasi-1D reacting flow problem, in order to highlight the main advantages of the proposed formulation.

Stagnation Line Flow

VKI has been involved for several years in the determination of catalytic properties of TPS materials. A hybrid methodology, which relies on the combination of experimental measurements and numerical calculations, has been employed for this purpose. The principles of this methodology lay on the local heat transfer simulation (LHTS) concept developed at the Institute for Problems in Mechanics of Moscow (IPM) [15]. Over the past few years, this methodology has been applied to both Mars and Earth atmospheric entry. This was possible thanks to both experimental measurements [28] and numerical tools [19,29–31] available at VKI, used together to compute the so-called heat flux maps needed to estimate the effective recombination probability of atoms and molecules on solid surfaces. From the numerical side, this requires the simulation of inductively coupled plasma flows plus the computation of stagnation line flows in front of the probe placed in the test chamber of the wind tunnel. In Fig. 1 we present a sketch describing the typical geometric configuration of standard tests/simulations conducted in the framework of the application of the methodology used at VKI.

The simulation of the flow in the torch and in the chamber is done assuming LTCE conditions and the results of this simulation are used to define the stagnation line differential problem. This is possible thanks to the computation of a set of nondimensional parameters used as inputs to rebuild the outer edge conditions to match the experimental heat flux. This iterative rebuilding process relies upon the simulation of the stagnation line flow of a mixture of reacting gases under chemical nonequilibrium assuming complete recombination at the wall. For the considered torch operating conditions, the concentrations of the ions rapidly decay away from the torch outlet allowing the description of the flow close to the probe by means of neutral species. After the outer edge conditions are rebuilt [32], a set of stagnation line nonequilibrium computations are performed to compute the wall heat flux as a function of wall temperature for several effective recombination probabilities. As shown in previous studies [5], assuming a fully catalytic wall provides a heat flux close to the one obtained by assuming LTCE conditions along the stagnation line, provided that elemental demixing is taken into account. Following this result, we identify the LTCE stagnation line problem as a suitable test case to present the main features of the formulation presented at the beginning of the paper. In addition, this will allow us to show how the analysis performed in [5], where the importance of demixing was assessed, is improved in terms of physical understanding of the flow behavior.

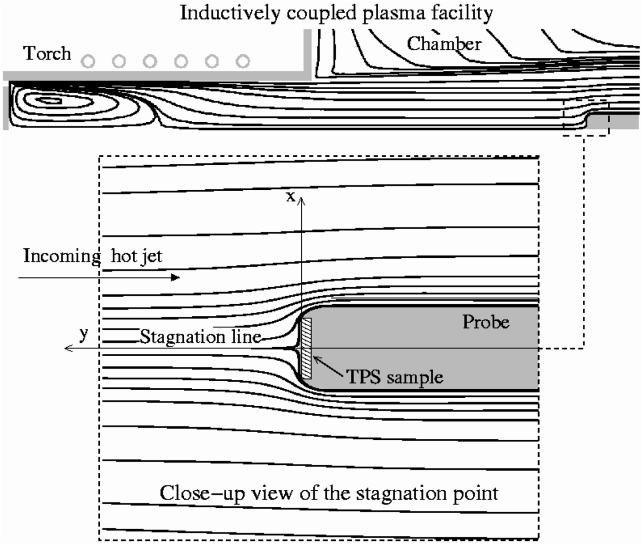

Fig. 1 Geometrical configuration.

To present our analysis of the stagnation line flow we will start defining a working mixture suited for the analysis of Martian entry problems. Further on, we will recall the stagnation line equations, and finally their solution will be presented with a strong emphasis on the description of diffusion phenomena.

Mixture Definition

Several models for the description of the Martian atmosphere are available in the literature. In [33], Noll and McElroy present detailed information on the atmospheric composition, and local information obtained from computations with climatological models is presented by Justus et al. [34] and Lewis [35]. As stated by Owen et al. [36], the atmosphere of Mars is mainly composed of CO_2, plus some N_2, O_2, Ar, and minor species. In this work by neglecting minor species and Ar, the Martian atmosphere is modeled with CO_2, N_2, and O_2. This choice was also adopted by Chen and Candler in [37], where hypersonic flow simulations are presented to predict the heat flux on a fore-body heat shield. We therefore consider an 8 species mixture defined as follows:

8-species Mars: $\mathcal{E} = \{\mathrm{C}, \mathrm{N}, \mathrm{O}\}$, $\mathcal{R} = \{\mathrm{CO_2}, \mathrm{CO}, \mathrm{O_2}, \mathrm{N_2}, \mathrm{NO}\}$.

In Fig. 2 we present the equilibrium composition of such a mixture for the reference elemental fractions $X^\delta_{\mathrm{C}} = 0.32$, $X^\delta_{\mathrm{N}} = 0.04$, and $X^\delta_{\mathrm{O}} = 0.64$ and for a pressure of 7000 Pa used later on for the stagnation line flow solution.

Governing Equations

In this section the governing equations of a mixture of reacting gases for the stagnation line flow are recalled [18,19]. With respect to

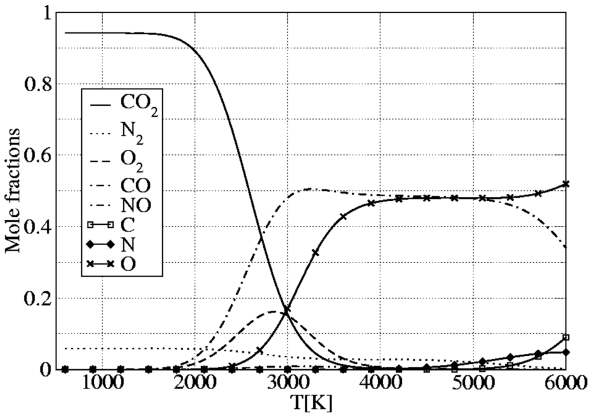

Fig. 2 Equilibrium mole fractions as a function of temperature (7000 Pa) [26].

previous formulations [5], the new formalism introduced in this paper will affect the form of the element continuity and energy equations. Indeed from Eq. (8), the diffusive fluxes of carbon, nitrogen, and oxygen read

$$\mathcal{J}_{\mathrm{C}} = -\rho D_{\mathrm{CC}} \nabla Y^{\mathrm{C}} - \rho D_{\mathrm{CN}} \nabla Y^{\mathrm{N}} - \rho D_{\mathrm{CO}} \nabla Y^{\mathrm{O}} - \rho D_{\mathrm{C}}^{T} \nabla T \quad (11a)$$

$$\mathcal{J}_{\mathrm{N}} = -\rho D_{\mathrm{NC}} \nabla Y^{\mathrm{C}} - \rho D_{\mathrm{NN}} \nabla Y^{\mathrm{N}} - \rho D_{\mathrm{NO}} \nabla Y^{\mathrm{O}} - \rho D_{\mathrm{N}}^{T} \nabla T \quad (11b)$$

$$\mathcal{J}_{\mathrm{O}} = -\rho D_{\mathrm{OC}} \nabla Y^{\mathrm{C}} - \rho D_{\mathrm{ON}} \nabla Y^{\mathrm{N}} - \rho D_{\mathrm{OO}} \nabla Y^{\mathrm{O}} - \rho D_{\mathrm{O}}^{T} \nabla T \quad (11c)$$

The direct consequence of these expressions is reflected on the heat flux vector which, in the absence of thermal and pressure diffusion, reads as follows:

$$\mathbf{q} = -(\lambda + \lambda_R + \lambda_D)\nabla T - \lambda_{\mathrm{EL}}^{\mathrm{C}} \nabla Y^{\mathrm{C}} - \lambda_{\mathrm{EL}}^{\mathrm{N}} \nabla Y^{\mathrm{N}} - \lambda_{\mathrm{EL}}^{\mathrm{O}} \nabla Y^{\mathrm{O}} \quad (12)$$

Hereafter we recall the main hypotheses on which the definition of the stagnation line differential problem is based. The flow is considered steady, axisymmetric, and laminar; the influence of body forces due to external fields is neglected; and finally, thermochemical equilibrium is supposed. Starting from a Cartesian reference system (Fig. 1) having the x axis lying on the body surface and the y axis normal to it, the Lees–Dorodnitsyn transformation

$$\xi(x) = \int_0^x \rho_\delta \mu_\delta u_\delta r^2 \, \mathrm{d}s \quad \text{and} \quad \hat{\eta} = \mathcal{K}\eta = \mathcal{K}\frac{u_\delta r}{\sqrt{2\xi}} \int_0^y \rho \, \mathrm{d}t$$

where

$$\mathcal{K} = \frac{1}{\delta}\frac{\sqrt{2\xi}}{u_\delta r} \int_0^{\hat{\eta}_{\max}} \frac{1}{\rho} \, \mathrm{d}\hat{\eta}$$

is applied. Three new independent variables are introduced as

$$F = \frac{u}{u_\delta}, \quad \theta = \frac{T}{T_\delta}, \quad \text{and} \quad \tilde{V} = \mathcal{K}\frac{2\xi}{\partial\xi/\partial x}\left(F\frac{\partial\eta}{\partial x} + \frac{\rho v r}{\sqrt{2\xi}}\right)$$

where δ is the boundary layer thickness, and r the local radius of the body. Therefore the stagnation line equations read as follows [5,19,38]:

Continuity:

$$\frac{\partial \tilde{V}}{\partial \hat{\eta}} + F = 0 \quad (13)$$

Momentum:

$$\tilde{V}\frac{\partial F}{\partial \hat{\eta}} = \frac{1}{2}\frac{\rho_\delta}{\rho}\left[1 + \frac{v_\delta}{(\partial u_\delta/\partial x)^2}\frac{\partial}{\partial y}\left(\frac{\partial u_\delta}{\partial x}\right)\right] - \frac{F^2}{2} + \frac{\partial}{\partial \hat{\eta}}\left(\mathcal{K}^2 l_0 \frac{\partial F}{\partial \hat{\eta}}\right) \quad (14)$$

Element continuity:

$$\tilde{V}\frac{\partial Y^e}{\partial \hat{\eta}} = \frac{-\mathcal{K}}{\sqrt{2\rho_\delta \mu_\delta \, \mathrm{d}u_\delta \, \mathrm{d}x}}\frac{\partial \mathcal{J}_e}{\partial \hat{\eta}} \qquad (e \in \mathcal{E}) \quad (15)$$

or, using Eq. (8),

$$\rho^2 D_{ee}\frac{\partial^2 Y^e}{\partial \hat{\eta}^2} = \left(\frac{\tilde{V}}{\chi} - \frac{\partial \rho^2 D_{ee}}{\partial \hat{\eta}}\right)\frac{\partial Y^e}{\partial \hat{\eta}} - \frac{\partial}{\partial \hat{\eta}}\left(\rho^2 D_e^T \frac{\partial T}{\partial \hat{\eta}}\right) - \frac{\partial}{\partial \hat{\eta}}\left(\rho^2 \sum_{q \neq e} D_{eq}\frac{\partial Y^q}{\partial \hat{\eta}}\right) \quad (16)$$

where the parameter $\chi = \mathcal{K}^2/(\mu_\delta \rho_\delta)$ is the result of the finite thickness assumption.

Energy:

$$\tilde{V}\frac{\partial \theta}{\partial \hat{\eta}} = -\tilde{V}\sum_{i \in \mathcal{S}}\frac{h_i}{h_{fr}}\frac{\partial y_i}{\partial \hat{\eta}} + \frac{1}{h_{fr}}\frac{\partial}{\partial \hat{\eta}}\left[\mathcal{K}^2\frac{\ell_0}{Pr}\frac{h_{fr}}{\lambda}(\lambda + \lambda_R + \lambda_D)\frac{\partial \theta}{\partial \hat{\eta}}\right] + \frac{1}{h_{fr}}\frac{\partial}{\partial \hat{\eta}}\left[\mathcal{K}^2\frac{\ell_0}{Pr}\frac{h_{fr}}{\lambda T_\delta}\sum_{q \in \mathcal{E}}\lambda_{\mathrm{EL}}^q \frac{\partial Y^q}{\partial \hat{\eta}}\right] \quad (17)$$

where $\ell_0 = \rho\mu/(\rho_\delta \mu_\delta)$, $Pr = \mu C_{p_{fr}}/\lambda$, $C_{p_{fr}} = \sum_{i \in \mathcal{S}} y_i \partial h_i/\partial T$, and $h_{fr} = C_{p_{fr}} T_\delta$.

Boundary conditions: The boundary conditions for the transformed variables are as follows. At the wall $F = 0$ and $\theta = T_w/T_\delta$, while at the outer edge $F = 1$ and $\theta = 1$. On the other hand, the boundary conditions for the physical variables are at the wall $u = 0$, $v = 0$, $T = T_w(x)$, while at the outer edge $u = u_\delta(x)$, $T = T_\delta(x)$, and $Y^e = Y_\delta^e(x)$.

The boundary condition for elements at the wall follows directly from mass conservation, that is, $\mathcal{J}_e = 0$ for $e \in \mathcal{E}$, since no new elements are generated in the surface chemistry (nonablative wall). From Eqs. (8–11), we see that for each element, the straightforward expressions for the diffusive fluxes are well suited for the numerical implementation of these boundary conditions. Indeed for each element, the mass conservation at the surface reads

$$\rho D_{ee}\left.\frac{\partial Y^e}{\partial \hat{\eta}}\right|_w = \rho D_e^T \frac{\partial T}{\partial \hat{\eta}} - \rho \sum_{q \neq e} D_{eq}\left.\frac{\partial Y^q}{\partial \hat{\eta}}\right|_w \qquad (e \in \mathcal{E}) \quad (18)$$

The previous expression represents a linear system for the gradients of elemental fractions ($\partial Y^e/\partial \hat{\eta}$). As a consequence, the solution of this linear system allows one to express the wall value of elemental fraction gradients as a linear function of the temperature gradient, allowing for an explicit formulation of the boundary condition (18). From a numerical point of view, the solution of a linear system may be avoided by following an explicit approach, that is, computing the right-hand side of Eq. (18) using the solution unknowns known from the previous iterative step.

It is important to notice how advantageous [6] the use of Eq. (18) is from a numerical point of view. The implementation of this boundary condition would be substantially more difficult if the element diffusive fluxes were to be computed as a linear combination of the solutions of Eq. (6): in general, inner iterations are then needed to impose the boundary condition. Equations (13), (14), (16), and (17) represent a system of second order ordinary differential equations which have been solved using a fourth-order finite difference discretization method [19]. As far as numerical accuracy is concerned, in [18] the authors showed that by using 100 points to discretize the stagnation line, grid convergence is achieved.

Table 1 Operating conditions

T_w, K	300
T_δ, K	5827
p_δ, Pa	7000
R_m, mm	25
δ, mm	0.9
$v_\delta \partial/\partial y(\partial u_\delta/\partial x)/(\partial u_\delta/\partial x)^2$ [−]	1.77
$\partial u_\delta/\partial x$, s^{-1}	913

Therefore all results presented hereafter have been obtained using 100 equidistant grid points.

Test Case Definition

The flow conditions considered, characteristic of Martian entry [39], are presented in Table 1. The presented outer edge conditions and geometrical parameters have been determined from a detailed numerical study of the flowfield inside the inductively coupled plasma generator and test chamber of the VKI's plasmatron wind tunnel [28] (Fig. 1). This allows for the computation of some nondimensional parameters related to the stagnation line edge in terms of the boundary layer thickness, the axial velocity, and the velocity gradient, and further details about their definition are available in previous publications [32].

In the following a single chemical regime is considered, corresponding to LTCE with demixing (LTCE-VEF), where the flow is in thermochemical equilibrium and the composition is computed as a function of pressure, temperature, and local elemental fractions, obtained from the solution of the set of elemental continuity equations. Two formulations have been used.

LTCE-VEF (1): We obtain the elemental concentration by solving Eq. (15), where the element diffusive fluxes are computed as a linear combination of the species ones obtained as the solution of the Stefan–Maxwell equations [Eq. (6)]. The computed species diffusive fluxes are then used in the energy equation to evaluate the diffusive transport of enthalpy ($\sum J_s h_s$) [5].

LTCE-VEF (2): We obtain the elemental concentration by solving Eq. (16), where the thermal demixing and multicomponent diffusion coefficients are used to compute the element diffusive fluxes. Moreover, the alternative form of the energy balance, presented in Eq. (17) is used, introducing the correction to λ_R as well as the elemental heat transfer coefficients.

A Priori Estimation of the Elemental Fraction Profiles

Before presenting the solution of the stagnation line problem, we analyze the evolution of the multicomponent and thermal demixing diffusion coefficients computed as a function of temperature for a fixed pressure and several elemental compositions. This is done independently from the solution of the stagnation line flow equations, with the purpose of showing how the knowledge of these transport coefficients can help to predict a priori the effect of multicomponent diffusion on the elemental concentration profiles. To this end, we present, in Fig. 3, the elemental thermal demixing coefficients and, in Figs. 4–6, the elemental multicomponent diffusion coefficients.

In these figures we present results for different elemental compositions to investigate their sensitivity to elemental fraction variations. Three sets of elemental composition have been selected for this purpose perturbing by ±5% the reference oxygen and carbon elemental molar fractions. This leads to the following elemental concentrations:

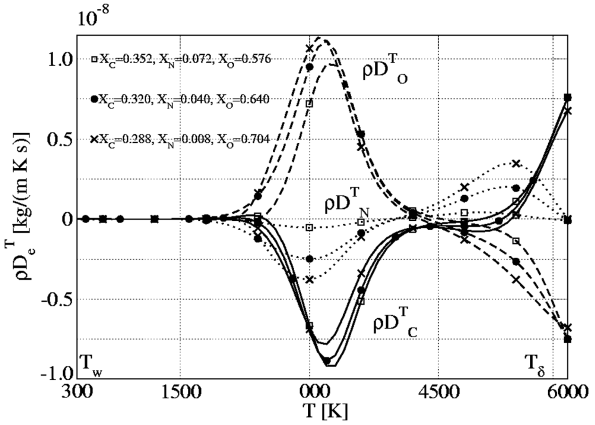

Fig. 3 Elemental thermal demixing coefficients as a function of temperature (7000 Pa).

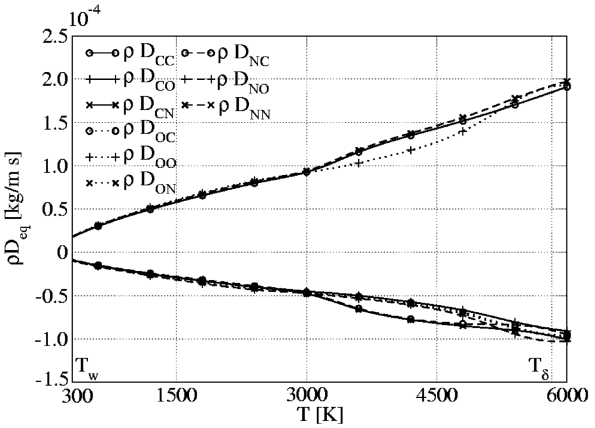

Fig. 4 Elemental multicomponent diffusion coefficients as a function of temperature (7000 Pa, $X_C = 0.352$, $X_N = 0.072$, $X_O = 0.576$).

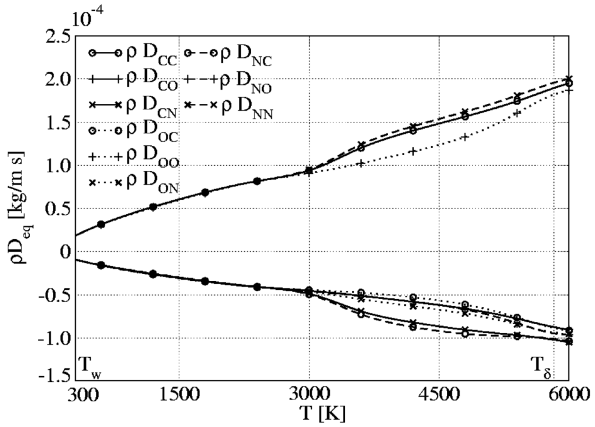

Fig. 5 Elemental multicomponent diffusion coefficients as a function of temperature (7000 Pa, $X_C = 0.320$, $X_N = 0.040$, $X_O = 0.640$).

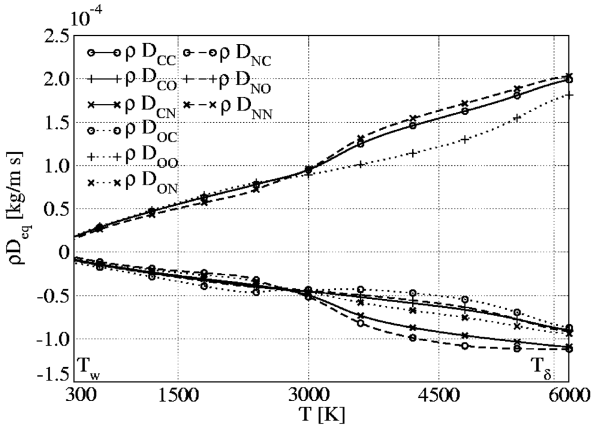

Fig. 6 Elemental multicomponent diffusion coefficients as a function of temperature (7000 Pa, $X_C = 0.288$, $X_N = 0.008$, $X_O = 0.704$).

$X_C = 0.352, X_N = 0.072, X_O = 0.576,$
$X_C = 0.320, X_N = 0.040, X_O = 0.640,$
$X_C = 0.288, X_N = 0.008, X_O = 0.704.$

The results presented in Fig. 3 show the influence of elemental fraction variations on the D_e^T. There we notice some differences between the results obtained with the three different elemental compositions even though the profile evolution as a function of temperature is analogous.

A different behavior is evident for the multicomponent diffusion coefficients presented in Figs. 4–6. There we observe a very similar behavior for the D_{eq} as a function of temperature for each elemental composition. From the definition of the stagnation line problem we know that the temperature increases from its wall value (set to a typical value ~300 K for cold wall) until the outer edge is reached where T_δ is ~6000 K. As a consequence, $\partial T/\partial y$ is a positive function of y. As shown in Fig. 3, the thermal demixing coefficients are not a positive function of T and present a change in sign in the temperature range $[T_w, T_\delta]$. This will obviously induce a similar change in sign in the demixing source terms $-\rho D_e^T \nabla T$. On the other hand, from Figs. 4–6 we notice how the elemental multicomponent diffusion coefficients do not change sign in the temperature range of interest. A further investigation of the multicomponent elemental diffusion coefficients reveals a particular structure of the diffusion matrix D_{eq}. Indeed, to respect mass conservation ($\mathcal{J}_e = 0$) the following conditions must be satisfied:

$$\sum_{q\in\mathcal{E}} D_{qC} = \sum_{q\in\mathcal{E}} D_{qN} = \sum_{q\in\mathcal{E}} D_{qO} \tag{19}$$

for the multicomponent diffusion coefficients, and

$$\sum_{e\in\mathcal{E}} D_e^T = 0 \tag{20}$$

for the thermal demixing ones. From the analytical definition of the D_{eq} [14] we moreover observe that the rows of the multicomponent diffusion coefficients matrix must sum up to zero ($\sum_{q\in\mathcal{E}} D_{eq} = 0$). This property is reflected by the results presented in Figs. 4–6 where we notice that the off diagonal coefficients have values around minus half of the diagonal ones. In addition the diagonal elements of the matrix follow approximately the same evolution as a function of temperature. Inspired by the previous two observations about the structure of the matrix of the D_{eq} we propose the following simplification of the multicomponent diffusion matrix:

$$[\rho D_{eq}] \approx \rho \frac{1}{2} \begin{bmatrix} 2D & -D & -D \\ -D & 2D & -D \\ -D & -D & 2D \end{bmatrix} \tag{21}$$

A rapid analysis of Eq. (21) reveals how both the physical mass constraint (19) and the mathematical property $\sum_{q\in\mathcal{E}} D_{eq} = 0$ are satisfied.

Equation (21), together with the identity $\sum \nabla Y^e = 1$, allows for a substantial simplification of the mixing term of the elemental diffusive fluxes, that is,

$$\sum \rho D_{eq} \nabla Y^q = \rho \frac{3}{2} D \nabla Y^e \tag{22}$$

Equation (22) represents an important result which shows that for CO_2/N_2 mixtures the mixing term $\sum \rho D_{eq} \nabla Y^q$ can be simplified to a Fick's law form which drops the coupling between the elemental continuity equations. Indeed, using Eq. (22) and considering steady flow conditions, the elemental continuity equation (9) simplifies to

$$\underbrace{\rho u \cdot \nabla Y^e}_{(1)} - \underbrace{\nabla \cdot (\rho \tfrac{3}{2} D \nabla Y^e)}_{(2)} = \nabla \cdot (\rho D_e^T \nabla T) \tag{23}$$

Equation (23), together with the profiles presented in Figs. 3–6, allows for the following qualitative prediction of the elemental fraction evolution along the stagnation line. Indeed, since at sufficiently low temperatures no chemical reactions take place, the D_e^T are zero and demixing of elements should not be induced in the region close to the surface. On the other hand, as temperature is sufficiently high, the demixing source terms $-\rho D_e^T \nabla T$ will differ from zero and, below ~4000 K, induce a decrease of oxygen concentration ($D_O^T > 0$) and an increase of N and C ($D_N^T, D_C^T < 0$). For higher temperatures the opposite effect will be observed. As soon as elemental concentrations vary, the terms $-\rho \sum D_{eq} \nabla Y^q$ will play a role trying to reestablish a uniform elemental composition. Moreover since the D_e^T change sign, while the D_{eq} do not, elemental fraction profiles should have a nonmonotonic behavior to produce zones where $\nabla Y^e > 0$ and others where $\nabla Y^e < 0$. In this way the terms $-\rho \sum D_{eq} \nabla Y^q$ try to counteract the demixing effect ($-\rho D_e^T \nabla T$).

In the remaining part of this section we propose an easy and fast method to estimate the elemental fraction evolution along the stagnation line. To this end we further simplify Eq. (23) neglecting the convective term (1) with respect to the mixing term (2). Although exact for a Couette flow, in the present case the accuracy of this approximation depends on the position along the stagnation line. The nondimensional parameter on which an accuracy analysis should be based is the Peclet number Pe resulting from the dimensional analysis of the ratio [(1)]/[(2)]. Indeed

$$\frac{[(1)]}{[(2)]} = \frac{v_\delta \delta}{\mathcal{D}} = Pe \tag{24}$$

where we introduced a reference velocity v_δ, a reference length δ, and a reference average diffusion coefficient $\mathcal{D}$. For the operating conditions defined in Table 1 we find a $Pe = 2$ which leads to a convective term (1) around the double of the mixing one (2). This clearly states that neglecting convection is not a good approximation in the zone around the outer edge. On the other hand, from Eq. (24), if the local velocity is used as a reference, we notice that as we move towards the surface the velocity normal to the wall decreases inducing a consequent decrease of the Peclet number. As a consequence, there will be an interval where the proposed approximation will be valid and, from the solution of the stagnation line problem to be presented shortly, we will notice that this interval covers the first 10% of the stagnation line. The direct consequence of neglecting convection in Eq. (23) consists in their simplification to the conditions $\mathcal{J}_e = 0$.

Following this result we propose an approximate approach to estimate the elemental composition along the stagnation line which consists in solving the following set of N_c decoupled first order ordinary differential equations:

$$\frac{\partial Y^e}{\partial \hat{\eta}} = -\frac{2}{3} \frac{\rho D_e^T}{\rho D} \frac{\partial T}{\partial \hat{\eta}} \tag{25}$$

As a first guess we consider a linear temperature distribution with slope $\partial T/\partial \hat{\eta} = (T_\delta - T_w)/\Delta\hat{\eta}$. This allows for the solution of Eq. (25) which leads to the determination of the elemental mass fraction profiles $Y^e(\hat{\eta})$. To solve Eq. (25) we have computed the $D_e^T[T(\hat{\eta})]$ and $D = D_{CC}[T(\hat{\eta})]$ using the outer edge pressure and elemental fractions.

In Fig. 7 we present the solution of Eq. (25) in terms of $Y^e(\hat{\eta})$. In this figure we present also the results obtained as the solution of Eq. (15) to compare the prediction of the method introduced in the previous section with the solution of the stagnation line equations. Analyzing the profiles presented in this figure we notice that the results of Eq. (25) lead to a prediction which differs from the solution of Eq. (15) ~2% at most, for oxygen near the wall. This result shows that the elemental fraction profiles can be estimated a priori with a reasonable accuracy using a fast and easy method.

In addition we notice that the evolution of the three profiles presented in Fig. 7 is in agreement with the qualitative prediction previously presented and moreover reflects the properties of the ratio D_e^T/D present in Eq. (25).

In the following section we will show how the results obtained with the approximate method just presented are not so different from the solution of the stagnation line equations. Indeed the evolution of

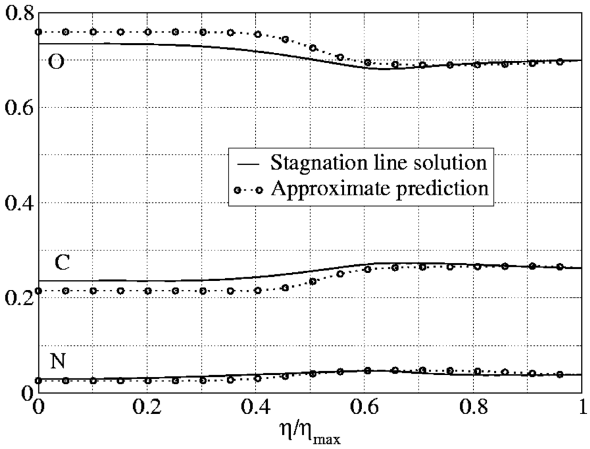

Fig. 7 Elemental mass fraction profiles obtained with an approximate method, compared to the full solution.

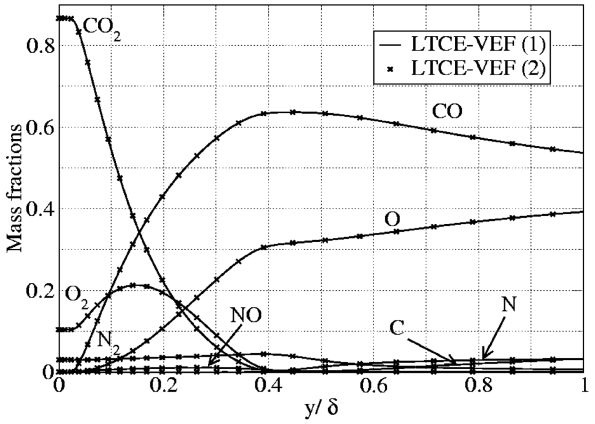

Fig. 9 Comparison of the computed results for the species mass fractions along the stagnation line using the LTCE-VEF (1) and the LTCE-VEF (2) formulations.

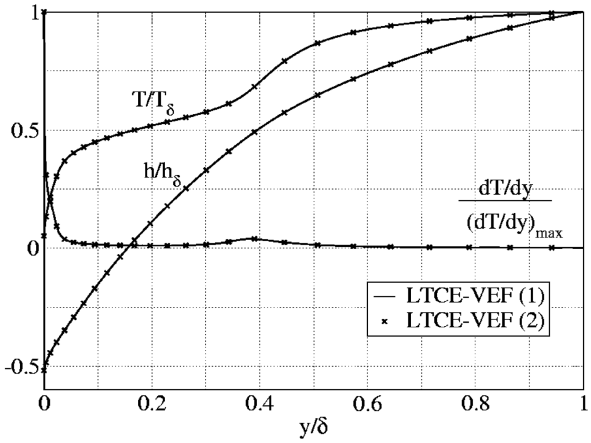

Fig. 8 Comparison of the computed results for the temperature and enthalpy profiles along the stagnation line obtained using the LTCE-VEF (1) and the LTCE-VEF (2) formulations.

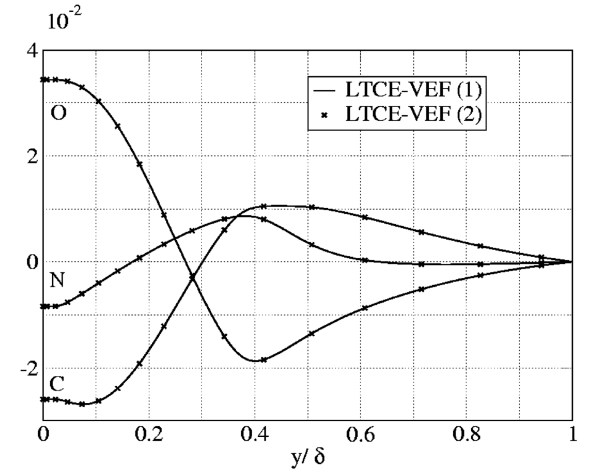

Fig. 10 Comparison of the results obtained for the difference between the elemental mass fractions and their outer edge values $[Y^e(y) - Y^e|_\delta]$ obtained using the LTCE-VEF (1) and the LTCE-VEF (2) formulations.

the D_e^T and the D_{eq} along the stagnation line will closely follow what has been presented in Figs. 3 and 5. This will allow researchers dealing with stagnation line problems for the TPS design to estimate a priori the order of magnitude of elemental fraction variations by means of a fast and easy tool.

Results

In this section we present the solution of the stagnation line equations for the conditions specified in Table 1. We start our analysis by discussing the temperature and enthalpy profiles shown in Fig. 8.

There we present the results obtained for the LTCE-VEF regime using the two formulations LTCE-VEF (1) and LTCE-VEF (2) defined in the previous section. As observed, the results obtained with the two formulations are identical. The same match is observed for all flow variables along the stagnation line, supporting the correctness of the alternative formulation recalled at the beginning of this paper.

In Fig. 9 we present the species concentration profiles. Starting from CO, O, C, and N at the outer edge, we see how their concentration decreases providing a mixture of CO_2, O_2, N_2 at the wall, and a small amount of NO. From the analysis of this picture, it appears that elemental demixing tends to reduce the amount of carbon and nitrogen at the wall while it enhances the oxygen concentration. This is reflected by the presence of an excess of O_2 in the low temperature region, which would have been zero if the wall elemental fractions had been the same as at the outer edge (Fig. 2). This behavior is confirmed by the profiles presented in Fig. 10, where we plot the difference between the local elemental mass fractions and their outer edge values $[Y^e(y) - Y^e|_\delta]$. In addition, by looking at the element concentration profiles (Fig. 10) we notice that the lack of carbon and nitrogen at the wall is compensated by a higher concentration around $y/\delta = 0.4$, whereas for oxygen we observe a minimum in this position from which the concentration rises until the wall is reached.

Going further with the analysis of the profiles presented in Fig. 10, we notice that they present a nonmonotonic behavior as already observed in [18] and here we give an explanation for this observation. To discuss the elemental mass fraction behavior we focus on the elemental continuity equations in the form of Eq. (15). It is clear how the knowledge of $\mathcal{J}_e$ will help in understanding the evolution of Y^e knowing that $\tilde{V} < 0$.

For this purpose we present the profiles of $\mathcal{J}_e$ in Fig. 11 for the three elements contained in the mixture. As expected [Eq. (15)] we observe a correspondence between the local extrema of $\mathcal{J}_e$ and those of Y^e. In addition we notice that the diffusive fluxes of elements are zero all over the first 10% of the stagnation line and they start to grow around $y/\delta \approx 0.1$. This shows that over the first 10% of the stagnation line, Eq. (15) simplifies to $\mathcal{J}_e = 0$, meaning that convection is negligible. Moving further towards the outer edge a local extrema is encountered followed by an increase for C and N, while for oxygen a decrease of $\mathcal{J}_O$ is observed. From this we notice that in the region defined by $y/\delta > 0.1$, the convective term will differ from zero and will counteract [Eq. (15)] the derivative of the profiles presented in Fig. 11. At this point it is important to observe that although the profiles of Fig. 11 allow for the interpretation of the

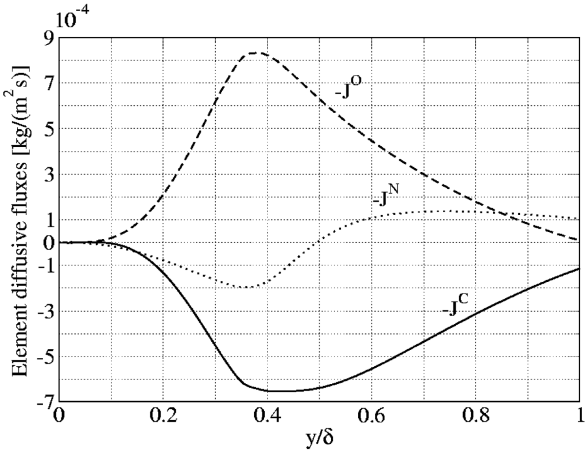

Fig. 11 Elemental diffusive fluxes ($-\mathcal{J}_e$).

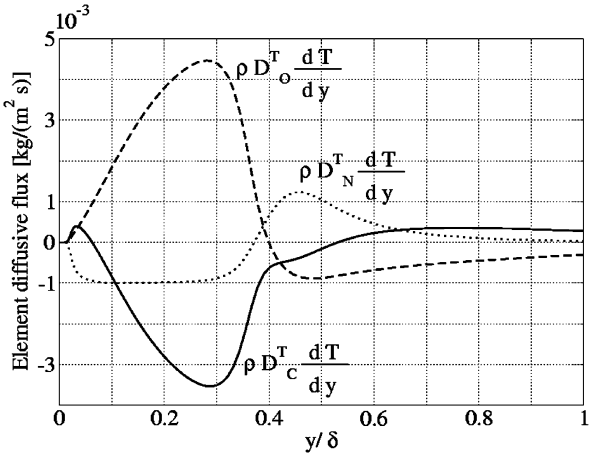

Fig. 12 First contribution to the element diffusive fluxes ($\rho D_e^T \nabla T$).

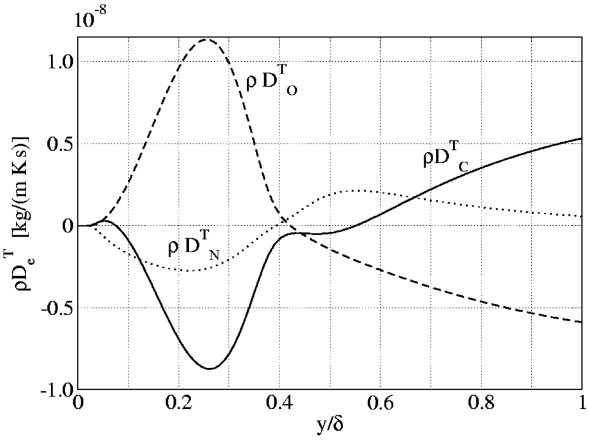

Fig. 13 Thermal demixing diffusion coefficients.

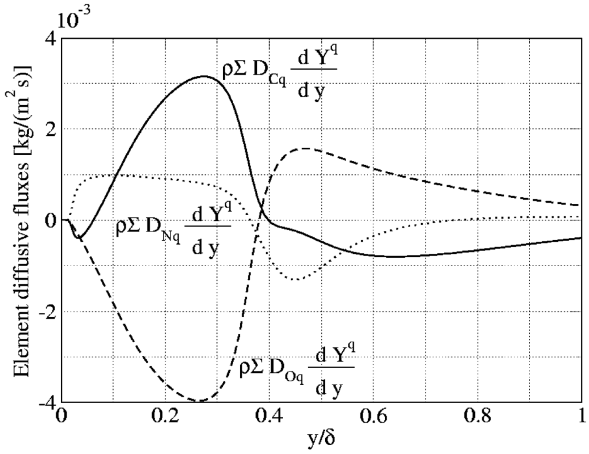

Fig. 14 Second contribution to the element diffusive fluxes ($\rho \sum D_{eq} \nabla Y^q$).

elemental fraction profiles presented in Fig. 10, it is by no means evident to give an explanation for the behavior of the $\mathcal{J}_e$ if they are computed as a linear combination of the solutions of Eq. (6) as done in the formulation LTCE-VEF (1) [5,6]. Now, to improve our understanding, we use the theory introduced in [14] and apply it in the LTCE-VEF (2) formulation of the equations.

Indeed, to understand the behavior of the element diffusive fluxes we discuss now the two components of $\mathcal{J}_e$. The first is proportional to the temperature gradient ($\rho D_e^T \nabla T$) and the second is obtained as a linear combination of the element mass fractions gradients ($\rho \sum D_{eq} \nabla Y^q$). In Fig. 12 we present the first part of the element diffusive fluxes. From Fig. 8 we notice that $\partial T/\partial y > 0 \quad \forall\ y$ and therefore the sign of $\rho D_e^T \nabla T$ will depend only on D_e^T, with ρ being obviously a positive quantity.

As shown in [14] and confirmed in Fig. 3, the D_e^T change their sign as temperature rises, for fixed pressure and elemental fractions. In the present case the pressure is constant along the stagnation line but the elemental fraction varies. Therefore both temperature and elemental composition will influence the transport properties. From the analysis conducted observing the results of Figs. 4–6, we expect the influence of temperature variations to be dominant with respect to changes in elemental composition. All these effects concur to the establishment of the profiles presented in Fig. 12.

Close to the wall the thermal demixing coefficients are zero and do not contribute to the element diffusive fluxes. As temperature rises we observe an increase in modulus of all contributions until a maximum is reached. Then we notice a decrease and a subsequent change in sign typical of the thermal demixing coefficients behavior.

Indeed from Fig. 13 we see how the behavior of the thermal demixing coefficients is similar to that of the first contribution to the element diffusive fluxes. At this point it is interesting to compare Figs. 3 and 13 remembering the nonlinear behavior of $T(y)$. At first glance we observe that the evolution of the D_e^T is mainly the same except for a slight increase of D_C^T observed close to the wall ($y/\delta \approx 0.05$) and absent when the elemental fraction is supposed to be constant (Fig. 3). The close relation between the results presented in these two figures, together with their importance in the understanding of diffusion phenomena, clearly shows the physical interest and the practical value of the computation of elemental thermal demixing coefficients.

In Fig. 14 we plot the second contribution to the elemental diffusive fluxes. Also this contribution starts from zero at the wall and follows a nonmonotonic behavior passing through a change in sign for O and C.

In Fig. 15 we notice how all the contributions to the sums $\rho \sum D_{eq} \nabla Y^q$ go through zero where the elemental fractions have a local minimum or maximum. The change in sign observed for the second contribution to the elemental diffusive fluxes is not due to the elemental multicomponent diffusion coefficients but to the elemental mass fractions. Indeed, as shown in [14] and observed in Figs. 4–6 and 16, the multicomponent diffusion coefficients have the same sign in the temperature range of interest.

This allows for the following interpretation of diffusion phenomena along the stagnation line. Because temperature decreases from the outer edge towards the wall, the temperature gradient is always positive along the stagnation line. In sufficiently low temperature regions, where chemical reactions do not occur, the thermal demixing coefficients are zero and do not induce demixing. As a consequence, since elemental multicomponent diffusion coefficients are not zero at low temperatures, the elemental composition stays constant ensuring mass conservation ($\mathcal{J}_e\,|_w = 0$). As we move away from the wall ($y < 0.05$) the thermal demixing

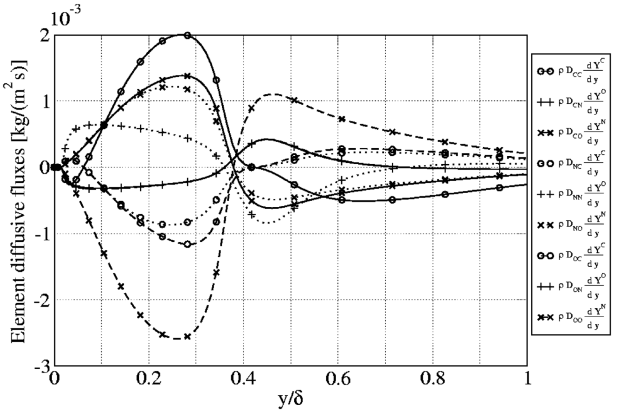

Fig. 15 Separate contributions to the element diffusive fluxes ($\rho D_{eq} \nabla Y^q$).

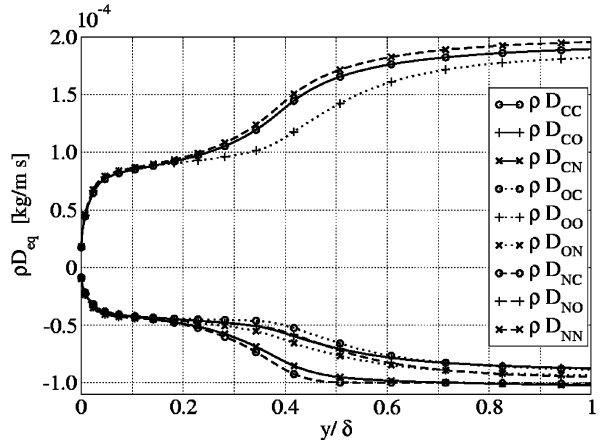

Fig. 16 Multicomponent elemental diffusion coefficients.

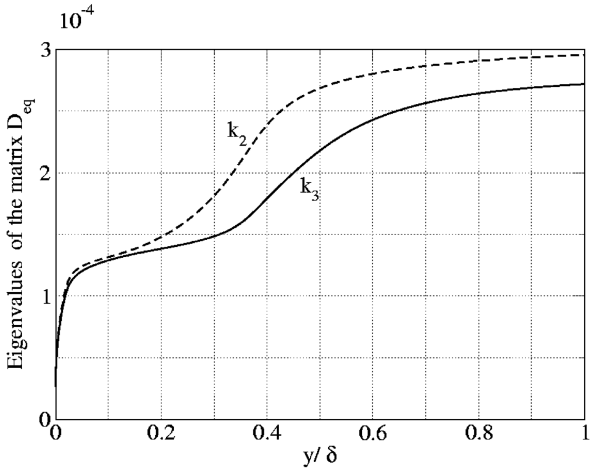

Fig. 17 Eigenvalues of the elemental multicomponent diffusion matrix along the stagnation line.

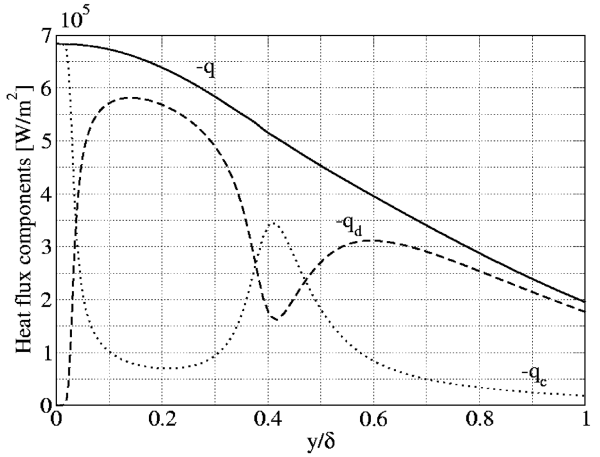

Fig. 18 Heat flux components.

coefficients cause a nonzero contribution to the elemental diffusion flux which tends to decrease oxygen concentration ($D_{\mathrm{O}}^T > 0$), increase nitrogen concentration ($D_{\mathrm{N}}^T < 0$), and slightly decrease but then increase again carbon concentration ($D_{\mathrm{C}}^T > 0$ and $D_{\mathrm{C}}^T < 0$). As soon as variations in elemental composition are induced ($\nabla Y^e \neq 0$), a counteracting contribution to the element diffusive fluxes starts to play a role trying to reduce demixing and inducing a reassessment of the element profiles until the outer edge is reached.

In the central part of the stagnation line, the two contributions to element fluxes interact until the point in which the thermal demixing coefficients change sign. There, to counteract this demixing term, the signs of element concentration gradients need to change because the multicomponent diffusion coefficients have a constant sign (Fig. 16). The counteracting character of the term $\sum \rho D_{eq} \nabla Y^q$ with respect to $\rho D_e^T \nabla T$ justifies its label of "mixing term" and the comparison of Figs. 12 and 14 clearly shows this behavior. The mathematical origin of this diffusive character of the mixing term has to be searched in the nonnegativity of the matrix containing the elemental multicomponent diffusion coefficients. To prove the latter property of the matrix D_{eq} we compute its eigenvalues along the stagnation line. Because this matrix is singular [$\sum_{q \in \mathcal{E}} D_{eq} = 0$], one eigenvalue is $k_1 = 0$ and the remaining two are presented in Fig. 17. There we clearly see that both k_2 and k_3 are positive $\forall\ y \in [0, \delta]$, this proving the nonnegative character of the matrix D_{eq}.

As a summary, we wish to point out that from the knowledge of the set of transport properties including both elemental thermal demixing and multicomponent diffusion coefficients such as those presented in Figs. 3–5, we can predict the evolution of the diffusive fluxes and therefore guess the shape of the elemental fraction profiles as well as the amount of demixing one should observe in the solution of the stagnation line problem.

We now move to the analysis of the heat and mass transfer along the stagnation line by means of conduction and diffusion. As shown at the beginning of the paper, under the assumption of local thermodynamic equilibrium, the diffusive transport of enthalpy can be split into two parts related to ∇T and ∇Y^q, respectively. As a consequence, as shown in Eq. (12), the computation of the heat flux involves the determination of two terms, one proportional to the temperature gradient $[-(\lambda + \lambda_R + \lambda_D)\nabla T]$ and the other proportional to the linear combination of element concentration gradients $[-\sum \lambda_{\mathrm{EL}}^q \nabla Y^q]$. Moreover, the heat flux in a mixture of reacting gases is composed of a conductive part ($\mathbf{q}_d = -\lambda \nabla T$), to which the diffusive transport of enthalpy needs to be added ($\mathbf{q}_d = \sum h_s J_s$). To investigate the heat flux along the stagnation line and highlight the relative importance of the various contributions we start presenting the evolution of $\mathbf{q}$, $\mathbf{q}_c$, and $\mathbf{q}_d$ along the stagnation line in Fig. 18.

There we observe that the total heat flux presents an increasing monotonic behavior starting from the outer edge until the wall, acting to balance the convection of enthalpy. At the same time we notice that this smooth evolution appears to be the result of a quite complex shape of the two contributions $\mathbf{q}_c$ and $\mathbf{q}_d$ presented in the same figure. This highly nonlinear behavior of the two heat flux components is the result of the evolution of six transport coefficients ($\lambda, \lambda_R, \lambda_D, \lambda_{\mathrm{EL}}^q$) and four gradients ($\nabla T, \nabla Y^q$). To provide an exhaustive description of the heat flux along the stagnation line we start investigating the behavior of the three thermal (λ), thermal reactive (λ_R), and demixing (λ_D) conductivities shown in Fig. 19.

As expected, we notice λ_R to be the major contribution to the first part of the heat flux followed by λ. We also notice that λ_D has a nonmonotonic behavior including changes in sign, highlighting the

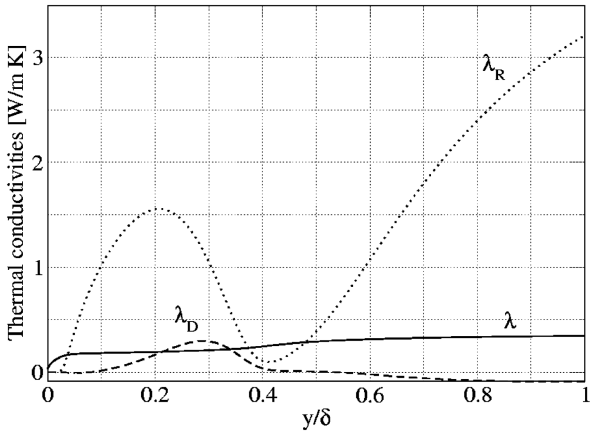

Fig. 19 Thermal, reactive, and demixing conductivities along the stagnation line.

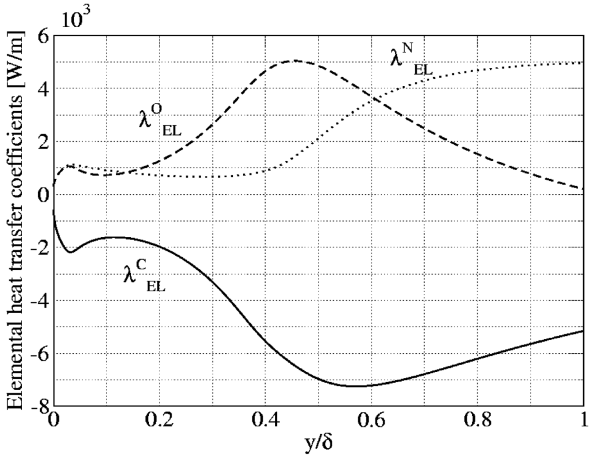

Fig. 21 Elemental heat transfer coefficients.

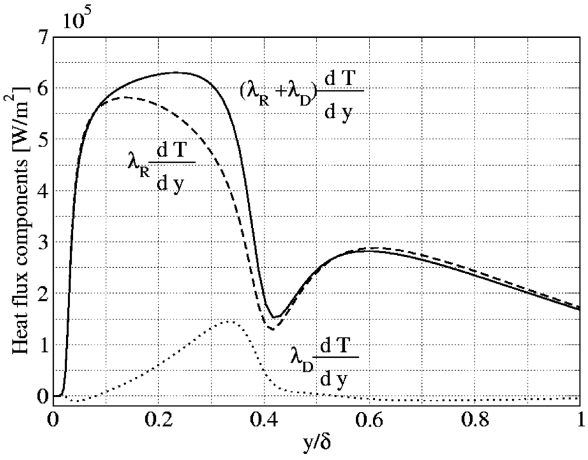

Fig. 20 Heat flux components ($\lambda_R \nabla T, \lambda_D \nabla T$) along the stagnation line.

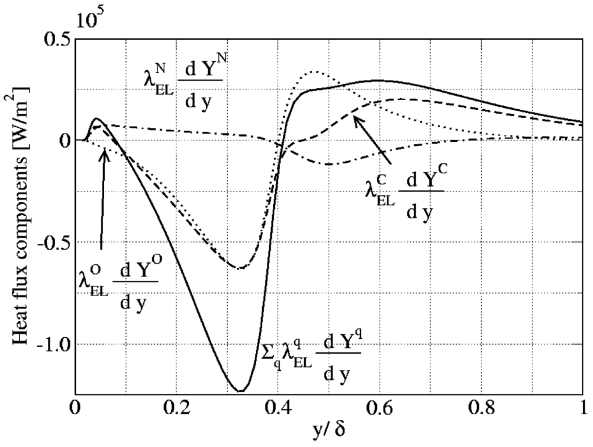

Fig. 22 Heat flux components ($\lambda^q_{\mathrm{EL}} \nabla Y^q$).

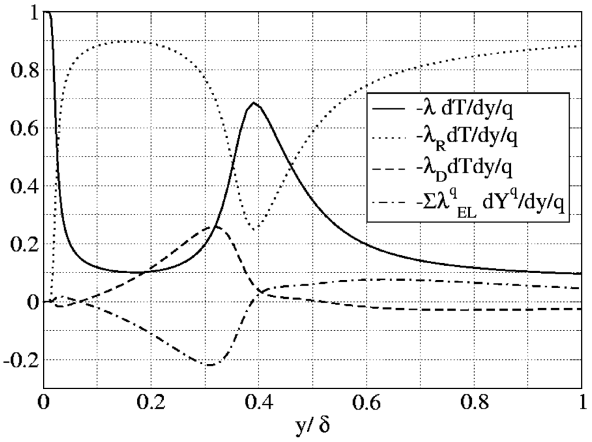

Fig. 23 Normalized heat flux components.

fact that demixing tends to increase or decrease heat flux depending on the local temperature and elemental fractions as already observed in [14]. Moreover, in terms of heat flux intensity, we notice that around $y/\delta = 0.3$, $\lambda_D \approx \lambda$ showing how, neglecting λ_D with respect to λ could lead to important errors. The knowledge of the evolution of the transport coefficients presented in Fig. 19 helps us understand the behavior of the various heat flux contributions. Indeed the nonlinear behavior of $\mathbf{q}_c$ can be easily explained. λ is an increasing monotone function from the wall towards the outer edge, while $\partial T/\partial y$ starting from the outer edge increases, decreases, and then increases again as shown in Fig. 8. Therefore $\mathbf{q}_c$ follows mainly the evolution of $\partial T/\partial y$. For what concerns $\mathbf{q}_d$ we need to consider separately the five contributions $-\lambda_R \nabla T$, $-\lambda_D \nabla T$, and $-\lambda^q_{\mathrm{EL}} \nabla Y^q$.

In Fig. 20 we present the evolution of the first two terms and their sum. The evolution of these two contributions is more complex than the previous one since the two associated transport coefficients present a highly nonlinear behavior with extrema in different positions than the temperature gradient. As far as the elemental heat transfer coefficients are concerned, we present their evolution in Fig. 21. There we notice that they all have a nonmonotonic behavior reflecting the highly reacting character of the flow. These transport coefficients lead to three contributions to the heat flux presented in Fig. 22 which are of the same order of magnitude for the three elements. The sum of these contributions is also plotted in the same figure to show the importance of this term with respect to the total heat flux. From the analysis of the profiles presented in Figs. 20–22, we can justify the evolution of $\mathbf{q}_d$ concurring to the determination of the final shape of the heat flux. As a final step we analyze in detail the relative importance of the various terms contributing to the heat flux. In Fig. 23 we present the results of this analysis showing the evolution of the four following ratios along the stagnation line: $-(\lambda\, \mathrm{d}T/\mathrm{d}y)/q$, $-(\lambda_R\, \mathrm{d}T/\mathrm{d}y)/q$, $-(\lambda_D\, \mathrm{d}T/\mathrm{d}y)/q$, and $-(\sum \lambda^q_{\mathrm{EL}}\, \mathrm{d}Y^q/\mathrm{d}y)/q$.

The analysis of these profiles helps us to quantify the importance of each term. Indeed this shows that the major contribution to the heat flux comes from the thermal reactive conductivity (λ_R), the second comes from conduction (λ), and the two remaining contributions are of the same order of magnitude. The analysis of the curve $-(\lambda_D\, \mathrm{d}T/\mathrm{d}y)/q$ reveals that the contribution related to elemental demixing is higher than the one due to thermal conductivity for $0.1 < y/\delta < 0.3$. The two contributions $-\lambda_D\, \mathrm{d}T/\mathrm{d}y$ and

$-\sum \lambda_{\mathrm{EL}}^{q}\, \mathrm{d}Y^{q}/\mathrm{d}y$ present almost an opposite behavior for $y/\delta < 0.4$. On the other hand, for $y/\delta > 0.4$ we notice that $-\sum \lambda_{\mathrm{EL}}^{q}\, \mathrm{d}Y^{q}/\mathrm{d}y$ becomes higher than $-\lambda_D\, \mathrm{d}T/\mathrm{d}y$ approaching the 10% of the total heat flux around $y/\delta \sim 0.6$ and decreasing to 5% at the outer edge. The almost opposite behavior of the two latter contributions clearly shows that elemental diffusive fluxes do not have a very important influence on the total heat flux. Indeed if $\mathcal{J}_e = 0 \quad \forall\, e \in \mathcal{E}$, the Butler and Brokaw thermal reactive conductivity is enough to compute $\mathbf{q}_d$. For the conditions previously analyzed, the presence of nonvanishing elemental fluxes acts on the mixture energetics behavior with a heat flux contribution which is at most of the order of 5% of the total heat flux.

Conclusions

The transport coefficients presented for a 8 species mixture containing three elements (C, N, O) under conditions of LTCE, allow one to reduce the equations of chemically reacting flows to an elegant system consisting of the conventional Navier–Stokes equations (mass, momentum, energy), complemented by an advection–diffusion equation for the mass fraction of each chemical element in the mixture. In the obtained formalism the diffusive fluxes are explicitly expressed in terms of gradients of the solution unknowns, unlike other formulations in which these fluxes are obtained in an implicit manner by solving the full system of Stefan–Maxwell equations. Several new LTCE transport coefficients appear:

1) The elemental advection–diffusion equations contain nine elemental multicomponent and three thermal demixing coefficients. The thermal demixing coefficients sum up to zero and the matrix of elemental multicomponent diffusion coefficients is nonsymmetric and nonnegative.

2) In the energy equation, the well-known thermal reactive conductivity coefficient (due to Butler and Brokaw) takes into account diffusive transport of species enthalpies in the absence of elemental demixing. An additional demixing thermal conductivity coefficient and a set of three elemental heat transfer coefficients correct for the additional flow of heat due to elemental demixing caused by temperature and elemental fraction gradients, respectively.

A quasi-one-dimensional application of this formulation is proposed by means of the solution of the equations describing the flow of a mixture of reacting gases along a stagnation line. Both the theoretical description of the formulation and its application to a case of interest for Mars entry applications lead us to the following major conclusions:

1) For the first time thermal demixing and multicomponent diffusion coefficients as well as elemental heat transfer coefficients and thermal demixing conductivity have been computed for a mixture containing three elements. This proves the generality of the proposed formulation and clearly represents an improvement with respect to previous formulations available in the literature.

2) The results obtained with the proposed closed form of the equations coincide with those obtained using an implicit formulation previously presented by the authors, indicating the correctness of the new formulation.

3) The proposed approximate method for the estimation of the elemental fraction profiles allows one to predict the elemental concentration along the stagnation line in an easy way with a maximum absolute error below 2%.

4) Demixing of chemical elements gives rise to complex elemental concentration and heat flux patterns which can be easily explained by examining graphs of LTCE transport coefficients that arise from the new LTCE formulation.

References

[1] Sarma, G. S. R., "Physico-Chemical Modeling in Hypersonic Flow Simulation," *Progress in Aerospace Sciences*, Vol. 36, No. 3–4, 2000, pp. 281–349.

[2] Butler, J. N., and Brokaw, R. S., "Thermal Conductivity of Gas Mixtures in Chemical Equilibrium," *Journal of Chemical Physics*, Vol. 26, No. 6, 1957, pp. 1636–1643.

[3] Brokaw, R. S., "Thermal Conductivity of Gas Mixtures in Chemical Equilibrium: 2," *Journal of Chemical Physics*, Vol. 32, No. 4, 1960, pp. 1005–1006.

[4] Vasil'evskii, S. A., Kolesnikov, A. F., and Yakushin, M. I., "Mathematical Models for Plasma and Gas Flows in Induction Plasmatrons," *Molecular Physics and Hypersonic Flows*, edited by M. Capitelli, Kluwer, Dordrecht, The Netherlands, 1996, pp. 495–504.

[5] Rini, P., and Degrez, G., "Elemental Demixing Along both Air and Carbon Dioxide Stagnation Line Flows," *Journal of Thermophysics and Heat Transfer*, Vol. 18, No. 4, 2004, pp. 511–518.

[6] Rini, P., Vanden Abeele, D., and Degrez, G., "Elemental Demixing in Inductively Coupled Air Plasmas at High Pressures," *Journal of Thermophysics and Heat Transfer* (to be published); also AIAA Paper 2004-2472.

[7] Suslov, O. N., Tirsky, G. A., and Shchennikov, V. V., "Flows of Multicomponent Ionized Mixtures in Chemical Equilibrium. Description Within the Framework of the Navier–Stokes and Prandtl Equations," *Zhurnal Prikladnoi Mekhaniki i Tekhnicheskoi Fiziki*, No. 1, 1971.

[8] Tirsky, G. A., "Up-to-Date Gasdynamic Models of Hypersonic Aerodynamics and Heat Transfer with Real Gas Properties," *Annual Review of Fluid Mechanics*, Vol. 25, Jan. 1993, pp. 151–181.

[9] Tirsky, G. A., "The Hydrodynamic Equations for Chemically Equilibrium Flows of a Multielement Plasma with Exact Transport Coecients," *Journal of Applied Mathematics and Mechanics*, Vol. 63, No. 6, 1999, pp. 841–861.

[10] Murphy, A. B., "Combined Diffusion Coefficients in Equilibrium Mixtures of Dissociating Gases," *Journal of Chemical Physics*, Vol. 99, No. 2, 1993, pp. 1340–1343.

[11] Murphy, A. B., "Diffusion in Equilibrium Mixtures of Ionized Gases," *Physical Review E*, Vol. 48, No. 5, 1993, pp. 3594–3603.

[12] Murphy, A. B., "Demixing in Free-Burning Arcs," *Physical Review E*, Vol. 55, No. 6, 1997, pp. 7473–7494.

[13] Murphy, A. B., "Demixing due to Frictional Forces in an Electric Arc," *Physical Review Letters*, Vol. 73, No. 13, 1994, pp. 1797–1800.

[14] Rini, P., Abeele, D. V., and Degrez, G., "Closed Form for the Equations of Chemically Reacting Flows Under Local Thermodynamic Equilibrium," *Physical Review E*, Vol. 72, No. 1, 2005, pp. 011204–011216.

[15] Kolesnikov, A. F., "Extrapolation from High Enthalpy Tests to Flight Based on the Concept of Local Heat Transfer Simulation," *Measurements Techniques for High Enthalpy and Plasma Flows*, Vol. 8B, Rhode-St-Genèse, Belgium, Oct. 1999, pp. 1–14, VKI-LS.

[16] Ern, A., and Giovangigli, V., *Physica A (Amsterdam)*, Vol. 260, Nov. 1998, pp. 49–72.

[17] Vincenti, W. G., and Kruger, C. H., *Introduction to Physical Gas Dynamics*, Wiley, New York, 1965.

[18] Rini, P., Garcia, A., Magin, T., and Degrez, G., "Numerical Simulation of CO_2 Stagnation Line Flows with Catalyzed Surface Reactions," *Journal of Thermophysics and Heat Transfer*, Vol. 18, No. 1, 2004, pp. 114–121.

[19] Barbante, P. F., "Accurate and Efficient Modeling of High Temperature Nonequilibrium Air Flows," Ph.D. Thesis, von Karman Institute, Rhode-Saint-Genèse, Belgium, 2001.

[20] Kolesnikov, A. F., and Tirsky, G. A., "Equations for Partially-Ionized Multicomponent Mixtures of Gases, Employing Higher Approximations of Transport Transfer Coefficients," *Fluid Mechanics-Soviet Research*, Vol. 13, No. 4, July–Aug. 1984, published in Russian in 1982.

[21] Ferziger, J. H., and Kaper, H. G., *Mathematical Theory of Transport Processes in Gases*, North-Holland, Amsterdam, 1972.

[22] Vasil'evskii, S., Sokolova, I., and Tirsky, G., "Determination and Calculation of the Effective Transport Coefficients for Chemically Equilibrium Flows of Partially Dissociated and Ionized Mixtures of Gases," *Zhurnal Prikladnoi Mekhaniki i Tekhnicheskoi Fiziki*, Vol. 1, 1986, pp. 68–79.

[23] Magin, T., and Degrez, G., "Transport Algorithms for Partially Ionized and Unmagnetized Plasmas," *Journal of Computational Physics*, Vol. 198, No. 2, 2004, pp. 424–449.

[24] Bottin, B., Vanden Abeele, D., Carbonaro, M., Degrez, G., and Sarma, G. S. R., "Thermodynamic and Transport Properties for Inductive Plasma Modeling," *Journal of Thermophysics and Heat Transfer*, Vol. 13, No. 3, 1999, pp. 343–350.

[25] Magin, T., Degrez, G., and Sokolova, I., "Thermodynamic and Transport Properties of Martian Atmosphere for Space Entry Application," AIAA Paper 2002-2226, 2002.

[26] Baumgart, J., Magin, T., Rini, P., Degrez, G., and Chazot, O., "Simulation of Entry in the True Mars Atmosphere," *Proceedings of the*

Fifth European Symposium on Aerothermodynamics for Space Vehicles, ESA Publications Division, 2004, ISBN 9290928743.

[27] Baumgart, J., "Simulation of Entry in the True Mars Atmosphere," Technical Rept. von Karman Institute for Fluid Dynamics, Rhode-Saint-Genèse, Belgium, VKI PR 2003-30, 2004.

[28] Bottin, B., Carbonaro, M., Chazot, O., Degrez, G., Vanden Abeele, D., Barbante, P. F., Paris, S., Vanderhaegen, V., Magin, T., and Playez, M., "The Plasmatron and Beyond: A Decade of Aerothermal Plasma Testing at the von Karman Institute," *26th International Conference on Phenomena in Ionized Gases (ICPIG 2003)*.

[29] Bottin, B., "Aerothermodynamic Model of an Inductively-Coupled Plasma Wind Tunnel," Ph.D. Thesis, von Karman Institute, Rhode-Saint-Genèse, Belgium, 1999.

[30] Vanden Abeele, D., "An Efficient Computational Model for Inductively Coupled Air Plasma Flows under Thermal and Chemical Non-Equilibrium," Ph.D. Thesis, von Karman Institute, Rhode-Saint-Genèse, Belgium, 2000.

[31] Magin, T., "A Model for Inductive Plasma Wind Tunnels," Ph.D. Thesis, von Karman Institute for Fluid Dynamics, St.-Genesius-Rode, Belgium, June 2004.

[32] Degrez, G., Barbante, P., de la Llave, M., Magin, T., and Chazot, O., "Determination of the Catalytic Properties of TPS materials in the VKI ICP Facilities," *ECCOMAS Computational Fluid Dynamics Conference 2001*, Publisher, City, 4–7 Sept. 2001, pp. 162–167.

[33] Noll, R. B., and McElroy, M. B., "Models of Mars' Atmosphere," space vehicle design criteria, SP-8010, NASA, Dec. 1974 (revised).

[34] Justus, C. G., and Johnson, D. L., "Mars Global Reference Atmospheric Model," NASA TR TM-2001-210961, 2001.

[35] Lewis, S. R., Collins, M., Forget, F., and Wanherdrick, Y., "Mars Climate Database v3.1—user manual," TR ESTEC, 2001.

[36] Owen, T., Biemann, K., Rushneck, D. R., Biller, J. E., Howarth, D. W., and Lafleur, A. L., "The Composition of the Atmosphere at the Surface of Mars," *Journal of Geophysical Research*, Vol. 82, No. 28, 1977, pp. 4635–4639.

[37] Chen, Y.-K., and Candler, G. V., "Navier Stokes Solutions with Surface Catalysis for Martian Atmospheric Entry," *Journal of Spacecraft and Rockets*, Vol. 30, No. 1, 1993, pp. 32–42.

[38] Barbante, P. F., Degrez, G., and Sarma, G. S. R., "Computation of Nonequilibrium High-Temperature Axisymmetric Boundary-Layer Flows," *Journal of Thermophysics and Heat Transfer*, Vol. 16, No. 4, 2002, pp. 490–497.

[39] Rini, P., Vasil'evskii, S. A., Kolesnikov, A. F., Chazot, O., and Degrez, G., "CO_2 Stagnation Line Flow Simulation for Mars Entry Applications," *38th AIAA Thermophysics Conference*, AIAA, Reston, VA, 2005.